Chinese Chemical Letters 31 (2020) 3121–3126

Contents lists available at ScienceDirect

Chinese Chemical Letters

journal homepage: www.elsevier.com/locate/cclet

Communication

LHRH/TAT dual peptides-conjugated polymeric vesicles for PTT enhanced chemotherapy to overcome hepatocellular carcinoma

Yu Qin[1], Qing Guo[1], Shengjie Wu, Chenlu Huang, Zhiming Zhang, Li Zhang, Linhua Zhang*, Dunwan Zhu*

Tianjin Key Laboratory of Biomedical Materials, Key Laboratory of Biomaterials and Nanotechnology for Cancer Immunotherapy, Institute of Biomedical Engineering, Chinese Academy of Medical Sciences & Peking Union Medical College, Tianjin 300192, China

ARTICLE INFO

Article history:
Received 3 March 2020
Received in revised form 11 June 2020
Accepted 15 June 2020
Available online 16 June 2020

Keywords:
Redox-responsive
Polymeric vesicles
Chemotherapy
Photothermal therapy
Combination therapy

ABSTRACT

Combination therapy such as photothermal therapy (PTT) enhanced chemotherapy is regarded as a promising strategy for cancer treatment. Herein, we developed redox-responsive polymeric vesicles based on the amphiphilic triblock copolymer PCL-ss-PEG-ss-PCL. To avoid the limited therapeutic effect of chemotherapeutic drugs caused by systemic exposures and drug resistance, the redox-sensitive polymeric vesicles were cargoed with two chemotherapeutics: doxorubicin (DOX) and paclitaxel (PTX). Besides, indocyanine green (ICG) was encapsulated, and cell-penetrating peptides and LHRH targeting molecule were modified on the surface of polymeric vesicles. The results indicated that the polymeric vesicles can load different kinds of drugs with high drug loading content, trigger drug release in responsive to the reductive environment, realize high cellular uptake *via* dual peptides and laser irradiation, and achieve higher cytotoxicity *via* chemo-photothermal combination therapy. Hence, the redox-responsive LHRH/TAT dual peptides-conjugated PTX/DOX/ICG co-loaded polymeric micelles exhibited great potential in tumor-targeting and chemo-photothermal therapy.

Hepatocellular carcinoma (HCC), the most frequent primary liver cancer, ranks second in cancer-related mortality because of ineffective therapy [1]. Appropriately formulated synergistic therapies may achieve better anticancer efficacy while minimizing the side effects caused by each agent. Clinical research on cancer therapy has gradually shifted from monotherapy to combinational therapies [2–4]. Chemotherapeutics such as doxorubicin (DOX) and paclitaxel (PTX) are among the key therapeutic agents for the treatment of various solid tumors. Compared with single-drug therapy, the synergistic treatment of DOX and PTX effectively increases the rate of tumor regression and the survival rate of patients due to their different effects and mechanisms on cancer cells [5–7]. However, the nonspecific distribution and rapid clearance of these chemotherapeutics severely limit their clinical applications and inevitably cause systemic toxicity [8]. Therefore, more specific and efficient delivery approaches for therapeutic agents need to be developed.

In cancer drug therapy, understanding the tissue distribution of chemotherapeutic agents is important in optimizing the treatment regimen [9]. However, real-time monitoring of therapeutic drugs in tumor tissues is almost impossible [10]. The rapid development of nanotechnology has provided the possibility of assembling several types of therapeutic agents in the same carrier simultaneously, and formulating a multifunctional nano-delivery system for multimodal synergistic therapies [11–14]. A variety of nano-delivery systems have been exploited in cancer diagnosis and therapy, such as liposomes and polymersomes [15], metal-organic framework nanoparticles [16], mesoporous [17] and biomimetic nanoemulsions [18]. Among these vectors, polymersomes have proved to exhibit excellent drug loading efficiency and good biocompatibility [19] because these polymersomes not only have hydrophilic and hydrophobic layers to encapsulate various drugs, but also they exhibit promising tumor-targeting ability by EPR effect and surface decorations [20].

Indocyanine green (ICG), as one of the cyanine dyes, is the only near-infrared probe approved by the FDA for medical diagnosis and imaging. It is also a photothermal converter responding to near-infrared light. These properties make ICG popular in fluorescence imaging and photothermal therapy [21–23]. Importantly, ICG-based photothermal therapy could coordinate with chemotherapy

* Corresponding authors.
E-mail addresses: zhanglinhua@bme.pumc.edu.cn (L. Zhang), zhudunwan@bme.pumc.edu.cn (D. Zhu).
[1] These authors contributed equally to this work.

https://doi.org/10.1016/j.cclet.2020.06.023
1001-8417/

to overcome the limitation of monotherapy. However, *in vivo* applications of ICG have been limited because of its bio-environmental instability, nontarget specificity, tendency to assemble in aqueous media, and rapid elimination from the body [24,25]. Thus, exploring a proper vector to deliver ICG is urgently in need.

Cell-penetrating peptides (CPPs) are capable of delivering drugs into almost any live cells. Transactivator (TAT) is one of the CCPs that has shown fast endosomal or lysosomal escape and quick nuclear localization [26]. However, their nonspecific interactions caused by primary amines limits their application [27]. A tumor-targeting and microenvironment-responsive TAT-functionalized nanoplatform would be highly desirable in cancer treatment. Luteinising hormone-releasing hormone (LHRH) is a promising liver cancer cell-specific molecular probe [28], which could avoid the nonspecific cell-penetrating effect caused by TAT.

In this study, polymeric vesicles were constructed based on redox-responsive amphiphilic triblock copolymer PCL-ss-PEG-ss-PCL by using thin-film hydration and ultrasonic methods. The synthesis and characterization of the polymeric vesicles can be found in Supporting information. PCL-ss-PEG-ss-PCL could form nanoparticles with a hydrophilic core, a hydrophobic layer, and a hydrophobic shell due to the intra- and/or inter-molecular interactions of the amphiphilic copolymers in aqueous media. This carrier successfully encapsulated hydrophobic drug PTX, amphiphilic drug DOX, and photothermal conversion agent ICG (Fig. 1A). As shown in Fig. 1B, the fabricated PINPs mixtures were green transparent with opalescence. After incubated with DOX, the mixtures (named DPINPs) turned homogeneous reddish brown. These images indicated ICG and DOX were successfully loaded in polymeric vesicles, and the mixtures remained uniform dispersion and nanoscale liquid. The morphological structure of DPINPs was a typical sphere with uniform particle size (Fig. 1C). The blank nanoparticles (blank NPs) exhibited an apparent spherical "core-shell" morphology with bilayered lamellar structure (Fig. 1D). Size, size distribution as well as zeta potential were characterized by NanoZS Zetasizer. As shown in Fig. 1E, uniform DPINPs particles were synthesized with an average diameter of 232.47 ± 1.47 nm and narrow polydispersity (0.127). Besides, the size and polydispersity index of PINPs was 167.87 ± 1.87 nm and 0.116 respectively, which decreased by 64.6 nm than the size of DPINPs. The bigger size of DPINPs is attributed to the loading of hydrophilic DOX, and the zeta potentials also confirm this inference. As shown in Fig. 1F, the zeta potential of blank NPs was changed from -2.17 mV to -25.8 mV after loading PTX and ICG (PINPs), which demonstrated that the negatively charged ICG was loaded in nanoparticles successfully. Due to the positive electrical property of free DOX, DPINPs (-11.6 mV) exhibited lower electronegativity than PINPs (-23.87 mV). These negatively charged surfaces are expected to make polymeric vesicles stay long-term stability under aqueous media and more biocompatible *in vivo* [29]. The encapsulation efficiency (EE) of PTX, ICG, DOX in DPINPs were 86.9%, 96%, 13.55%, respectively, and the loading content (LC) was 8.9%, 9.86%, 2.06%, respectively, exceeding those of most current anti-cancer drug delivery carrier.

Since the concentration of reductive compounds (such as glutathione) in the intracellular matrix is much higher than the extracellular environment, disulfide bond based compounds appear to be promising candidates for intracellular delivery as these carriers can be specifically decomposed in the reductive environment [30–33]. The *in vitro* drug release of DOX and PTX from DPINPs in response to the reductive environment was further evaluated to confirm the redox sensitivity of this nanocarrier. Glutathione (GSH) with certain concentrations was used to imitate the intracellular reductive environment. Fig. 2A indicated that the release profile of DOX divided into sharp release and relaxedly

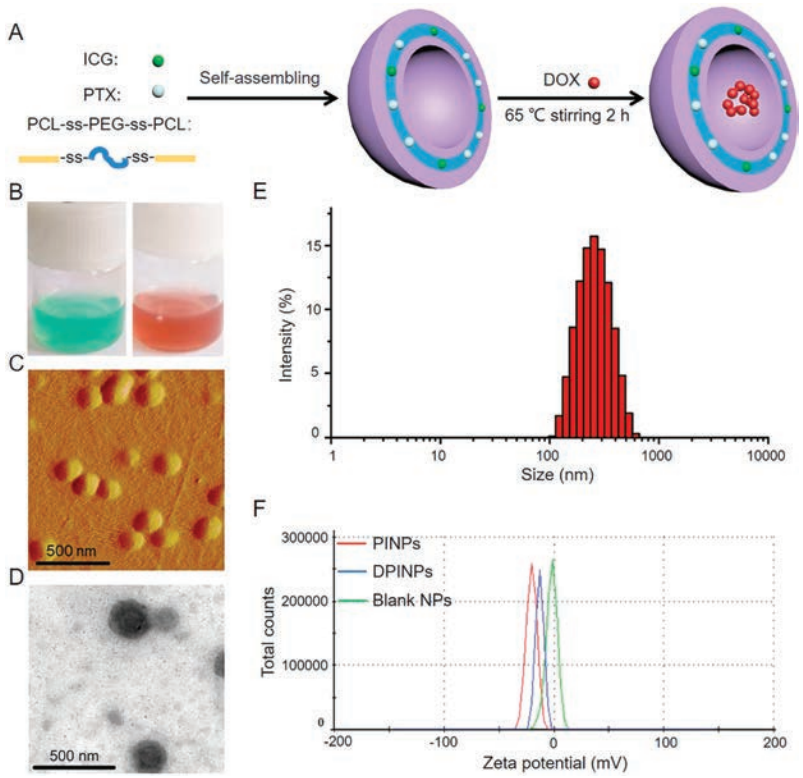

Fig. 1. Synthesis and characterization of polymeric vesicles. (A) Schematic illustration of the construction procedure of DPINPs; (B) Images of prepared drug-loaded polymeric vesicles before (displayed in green) and after (displayed in reddish brown) encapsulated DOX; (C) AFM images of DPINPs (scale bar: 500 nm); (D) TEM image of blank NPs (scale bar: 500 nm); (E) Size distribution of DPINPs; (F) Zeta potential of blank NPs, PINPs and DPINPs.

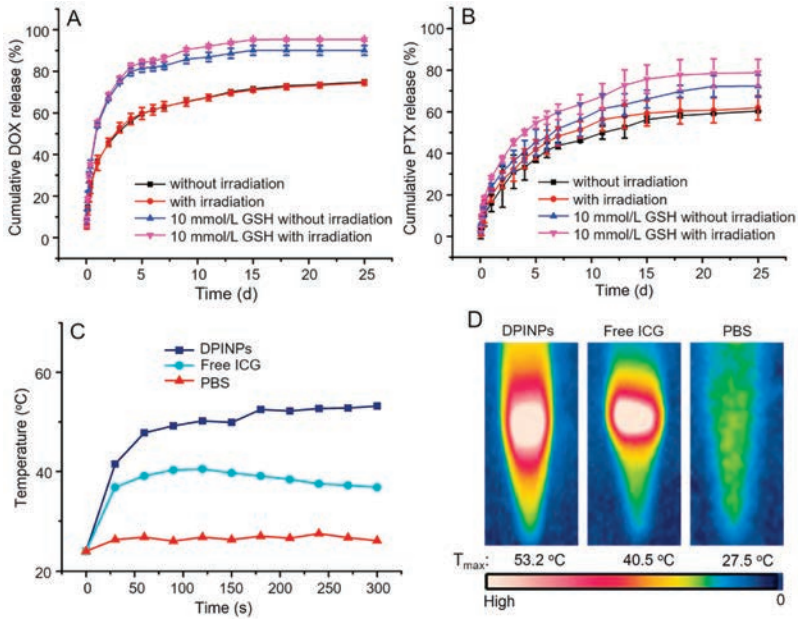

Fig. 2. *In vitro* drug release and photothermal effect of DPINPs: DOX (A) and PTX (B) release profile from the redox-sensitive polymeric vesicles in various conditions at 37 °C for 25 days; The temperature variation (C) and maximum temperature images (D) of the solutions of PBS, free ICG, and DPINPs, as a function of 5 min continuous 808 nm laser irradiation with the laser intensity of 1 W/cm^2.

release periods. At the initial stage of drug release, hydrophilic DOX released explosively. The adsorption behavior of positive DOX on the surface of DPINPs was responsible for the DOX burst release. After 48 h of release, the cumulative release rate of DOX in the simulated physiological conditions (expressed as without irradiation), laser irradiating (expressed as with irradiation), GSH simulated reductive condition (expressed as 10 mmol/L GSH without irradiation), and GSH solution with laser irradiating (expressed as 10 mmol/L GSH with irradiation) reached 45.26%, 45.81%, 66.69%, and 68.31%, respectively. Subsequently, the DOX release from DPINPs showed an obvious sustained release and the cumulative DOX release in GSH + laser condition exceeded 80% in 7 days. Laser irradiating did not significantly promote the DOX release, possibly because the speed of the initial burst release covered up the effect of laser. By contrast, the release behavior of PTX from DPINPs was a slow and continuous release without an initial burst effect. As shown in Fig. 2B, the release of PTX was significantly accelerated under a reducing environment (10 mmol/L GSH), and the laser irradiation also enhanced the drug release. These results indicate that this drug delivery system exhibit a redox-responsive and laser-responsive characteristics.

ICG is the typical NIR-absorbing PTT agent. To evaluate the *in vitro* photothermal effect of DPINPs, we monitored the laser-induced temperature variation of PBS, free ICG, and DPINPs by using an infrared thermal imaging camera (Figs. 2C and D). During 5-min irradiation, the temperature of DPINPs increased rapidly and the highest temperature reached 53.2 °C, while free ICG saw a swift growth in the first 30 s and slightly decrease subsequently. Due to the optical and chemical instability of free ICG in aqueous media, the maximum temperature of free ICG during irradiation only reached 40.5 °C. PBS buffer showed a small magnitude of the warming with the highest temperature of 27.5 °C, which illustrated that near-infrared laser irradiation could not induce temperature rising without a photothermal converting agent. The cause of the superior photothermal efficiency of DPINPs might lie in the fact that the shell of DPINPs could concentrate ICG and reduce heat dissipating. Thus, the thermo-therapeutical effect of ICG was maintained in the DPINPs and provided a basis for photothermal therapy.

Since both DOX and ICG are known to emit autofluorescence, CLSM could intuitively visualize the intracellular localization of DOX and ICG in BEL 7404 cells. To enhance the targeting and penetrating property of nano-carrier, LHRH and TAT peptide were modified on the surface of DPINPs. As shown in CLSM images (Figs. 3 and 4), The cell morphology and drug distribution changed with intervening formulations and laser irradiation. Normally, BEL 7404 cells were spindle-shaped or polygonal with uniform size, but after incubated with drug-loaded polymeric vesicles, cell turned short shuttle-like or round shape. Specifically, the cell membrane

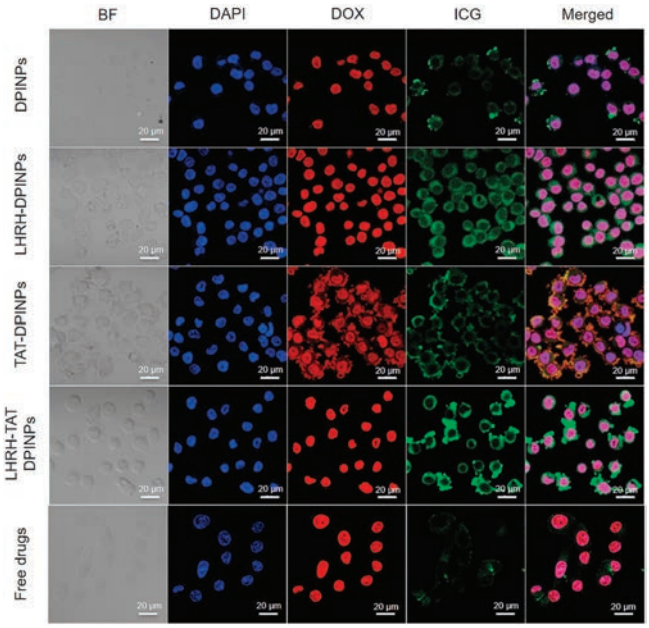

Fig. 3. Uptake of various formulations by BEL 7404 tumor cells. CLSM observation of the intracellular distribution of DPINPs, LHRH-DPINPs, TAT-DPINPs, LHRH-TAT DPINPs and free DOX&PTX&ICG in BEL 7404 cells after incubation for 4 h (scale bar: 20 μm).

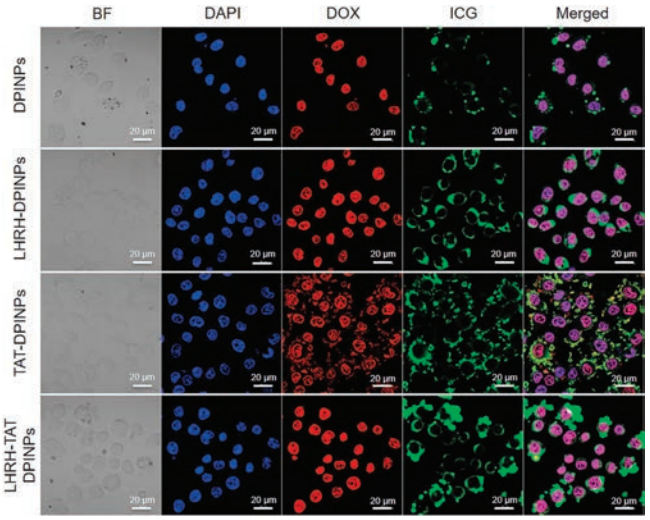

Fig. 4. Uptake of various formulations by BEL 7404 cells after laser irradiation. CLSM observation of the intracellular distribution of DPINPs, LHRH-DPINPs, TAT-DPINPs and LHRH-TAT DPINPs in BEL 7404 cells after laser irradiation and incubation for 4 h (scale bar: 20 μm).

became deformed and uncompleted after treated with TAT-DPINPs, which could be observed in the bright field (BF). The occurrence of this phenomenon was consistent with the cell-penetrating effect of TAT, thereby demonstrating cell-penetrating peptides modified polymeric vesicles could ferry much larger molecules into cells independent of classical endocytosis. Dox and ICG are prone to located in cell nucleus and cytoplasm respectively, as both drugs have their action mechanisms. As shown in Fig. 3, the fluorescence intensity of ICG in TAT-LHRH-DPINPs, LHRH-DPINPs, TAT-DPINPs, DPINPs, and free DOX&PTX&ICG treated cells appeared a decreasing trend, suggesting that TAT and LHRH decorations could enhance the internalization of drug-loaded polymeric vesicles. Unlike ICG internalization, free DOX was much easier to enter BEL 7404 cells than other formulations, which result from the rapid passive diffusion of hydrophilic DOX.

Besides, we investigated whether the laser irradiation could accelerate intracellular uptake. After laser irradiating (Fig. 4), the fluorescence intensity of DOX and ICG distributed in cells was much higher than each of the non-laser irradiating group, indicating ICG-induced photothermal effect can improve cellular uptake of drug-loaded polymeric vesicles, and accelerate drug release. Similarly, the highest fluorescence intensity of DOX and ICG in cells observed in LHRH-TAT DPINPs could be attributed to additional LHRH targeting, cell-penetrating effect, and ICG-induced hyperthermia.

The fluorescence intensity of intracellular DOX and ICG was further semi-quantitated by high-content cellular analysis system. As shown in Fig. 5, BEL 7404 cells were incubated with DPINPs, LHRH-DPINPs, TAT-DPINPs, LHRH-TATDPINPs and free DOX&PTX&ICG for 1 h, 4 h, and 24 h. Few DOX and ICG signals were detected in cells after 1-h incubation, whereas the internalization of both drugs enhanced when the incubation prolonged to 4 h. This correlation demonstrated that the internalization of those formulations was time-dependent. For free DOX treated cells, the DOX signal at 24 h decreased to 330.59 after an increase from 1 h (153.24) to 4 h (380.53), possibly because the transportation of free DOX was limited after passive diffusion had reached saturation. In comparison, the cellular uptake of DOX in polymeric vesicles treated groups increased with cultural time, indicating the superiority of fabricated nano-carrier. Both TAT and LHRH modifications improve the efficiency of drug delivery. For LHRH-TAT DPINPs treated cells after 4-h incubation, the fluorescence intensity of DOX in the nucleus and ICG in cytoplasm enhanced over 2.47 times and 24.24 times respectively after laser irradiation. This significant increase further indicated that the photothermal effect could accelerate the cell endocytosis of chemotherapeutic drugs.

Since increased cellular uptake is associated with enhanced cytotoxicity in tumor cells, cytotoxicities of different formulations against Bel 7404 cells were analyzed by MTT method. As shown in Fig. 6A, LHRH-TAT-NPs (LHRH-TAT modified blank carrier) exhibited high safety and biocompatibility towards BEL 7404 cells with carrier concentrations ranging from 0.243 μg/mL to 485.4 μg/mL, as over 90% of cell viabilities were observed in this group. Furthermore, the growth of BEL 7404 cells was significantly inhibited by DPINPs, LHRH-DPINPs, TAT-DPINPs, LHRH-TAT DPINPs, and free DOX&PTX in a dose-dependent way. Due to the sustainable release of LHRH-TAT-NPs, the cytotoxicity of LHRH-TAT-NPs had no vantage compared with free DOX&PTX after 24-h incubation. Free DOX enter cells through passive diffusion and could direct contact with tumor cell, causing higher *in vitro* toxicity than nanoparticles. compared with DPINPs, the higher cytotoxicity of LHRH-DPINPs implies that LHRH bonding significantly improved the targeting efficacy of nanoparticles to BEL 7404 cells lines. TAT modified polymeric vesicles (TAT-DPINPs) displayed more severe toxicity than DPINPs in different drug concentrations, which was consistent with the results of cellular uptake, demonstrating the cell-penetrating effect of TAT peptide could effectively improve the anti-cancer activity of nanoparticles.

To visualize the photothermal-induced cytotoxicity, live and dead BEL 7404 cells following 4-h cultivation with LHRH-TAT-

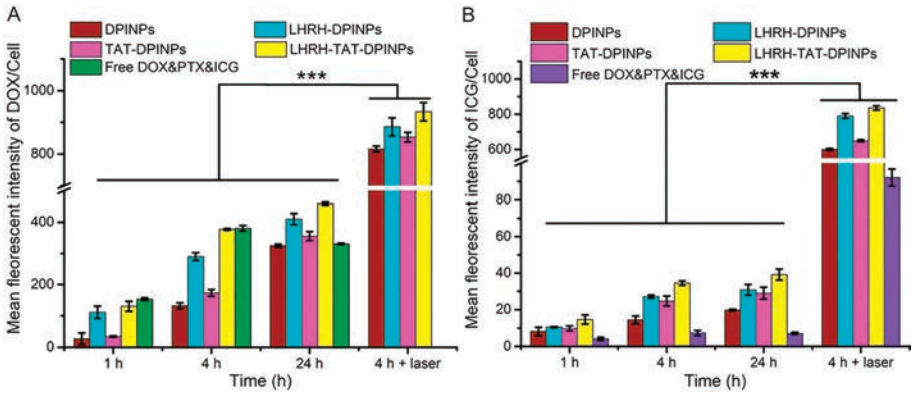

Fig. 5. Uptake of various formulations by BEL 7404 tumor cells. High-content cellular analysis of the mean fluorescence intensity of DOX and ICG in BEL-7404 cells after being incubated with different formulations for 1, 4 and 24 h. Data are presented as mean ± SD ($n = 6$).

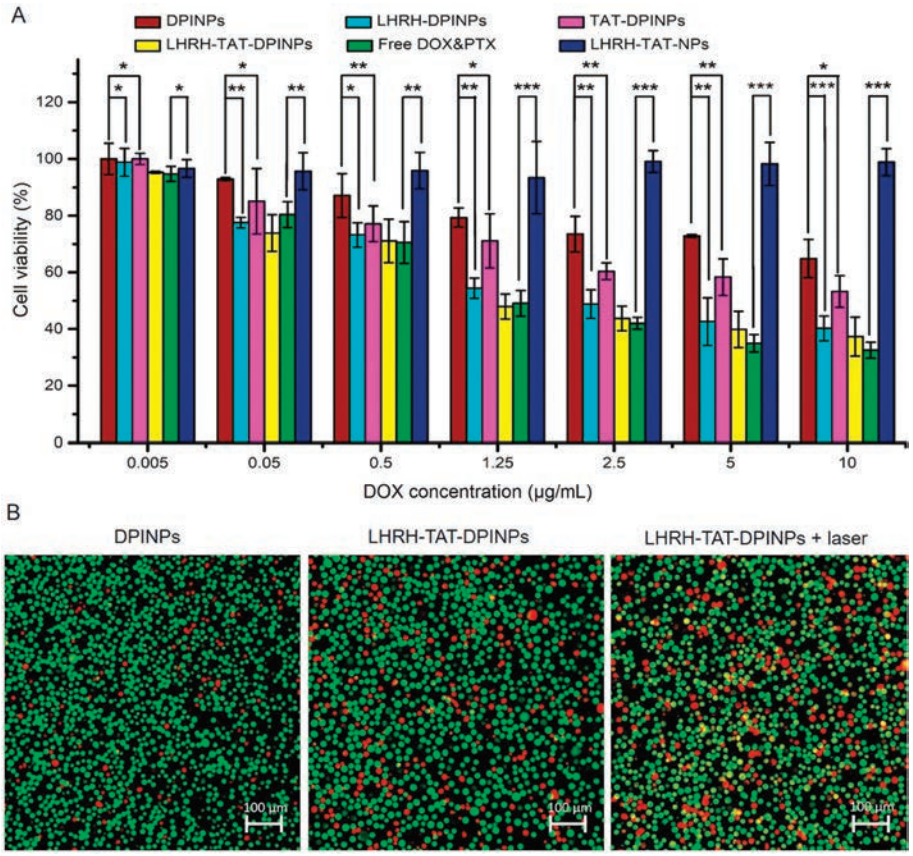

Fig. 6. (A) *In vitro* cytotoxicity analysis of BEL 7404 cells exposed to DPINPs, LHRH-DPINPs, TAT-DPINPs, LHRH-TAT-DPINPs, LHRH-TAT-NPs (LHRH-TAT modified blank carrier) and free DOX&PTX&ICG for 24 h. Data are presented as mean ± SD ($n = 6$). Significant differences: $^{*}P < 0.05$, $^{**}P < 0.01$ and $^{***}P < 0.001$. (B) CLSM images of BEL 7404 cells exposed to DPINPs, LHRH-TAT-DPINPs, LHRH-TAT-DPINPs + laser. Cells were stained with calcein-AM/PI living cell (green fluorescence)/dead cell (red fluorescence) kit after 4-h incubation.

DPINPs or DPINPs were imaged. Since the treatment duration against BEL 7404 was short, dead cells were sparsely seen in the DPINPs group. However, more dead cells were observed in LHRH-TAT-DPINPs with/without laser-treated groups, and LHRH-TAT-DPINPs + laser increased the proportion of dead cells (Fig. 6B). The results suggested a great targeting, cell-penetrating effect, PTT enhanced chemotherapy in BEL cells by LHRH-TAT-DPINPs + laser treatment.

In conclusion, a redox-sensitive amphiphilic copolymer PCL-ss-PEG-ss-PCL was constructed to achieve PTT enhanced chemotherapy and tumor-targeted effects by molecular self-assembly approach. The redox-sensitive multifunctional polymeric vesicles, which is specific for high glutathione (GSH) level in tumor cells, can release drugs *via* the cleavage of the disulfide bond. We obtained polymeric vesicles with homogeneous particle size distribution and good drug loading efficacy. The superior photothermal efficiency made DPINPs a promising formulation for PTT therapy. *In vitro* cellular uptake and cytotoxicity assays revealed that this drug delivery system has several advantages as follows: (1) Blank polymeric vesicles are good drug delivery carriers in terms of their good safety and biocompatibility; (2) The cellular drug accumulation increased with incubation durations owing to the sustainable release and long-term effects of nanoparticles; (3) DPINPs or surface-functionalized DPINPs can respond to laser irradiation, thereby generating hyperthermia to enhance cellular uptake and cytotoxicity of nanoparticles; (4) The modification of LHRH and TAT could optimize the carriers' targeting and penetrating effect towards BEL 7404 cells. Taken together, this drug delivery system provides a robust strategy for carrying multiple types of drugs, tumor targeting and penetrating, and achieve high anti-cancer effect *via* chemo-photothermal combination therapy.

Declaration of competing interest

The authors declare that they have no known competing financial interests or personal relationships that could have appeared to influence the work reported in this paper.

Acknowledgments

This work was supported by the National Natural Science Foundation of China (Nos. 81671806, 81571793), CAMS Initiative for Innovative Medicine (Nos. 2017-I2M-4-001, 2017-I2M-3-020), and Fundamental Research Funds for the Central Universities (Nos. 2019PT320028, 2019-0831-03).

Appendix A. Supplementary data

Supplementary material related to this article can be found, in the online version, at doi:https://doi.org/10.1016/j.cclet.2020.06.023.

References

[1] J.D. Yang, P. Hainaut, G.J. Gores, et al., Nat. Rev. Gastroenterol. Hepatol. 16 (2019) 589–604.
[2] O. Veiseh, F.M. Kievit, R.G. Ellenbogen, et al., Adv. Drug Deliv. Rev. 63 (2011) 582–596.
[3] W. Huang, L. Chen, L. Kang, et al., Adv. Drug Deliv. Rev. 115 (2017) 82–97.

[4] M.T. Piccolo, C. Menale, S. Crispi, Anticancer Agents Med. Chem. 15 (2015) 408–422.
[5] D.W. Zhu, S.J. Wu, C.Y. Hu, et al., Acta Biomater. 58 (2017) 399–412.
[6] Y. Wang, J. Wang, L. Yang, et al., Nanomedicine 21 (2019) 102066.
[7] J. Gehl, M. Boesgaard, T. Paaske, et al., Ann. Oncol. 7 (1996) 687–693.
[8] G.S. Karagiannis, J.S. Condeelis, M.H. Oktay, Cancer Res. 79 (2019) 4567–4576.
[9] S. Luo, E. Zhang, Y. Su, et al., Biomaterials 32 (2011) 7127–7138.
[10] S. Zanganeh, R. Spitler, G. Hutter, et al., Immunotherapy 9 (2017) 819–835.
[11] W. Fan, B. Yung, P. Huang, et al., Chem. Rev. 117 (2017) 13566–13638.
[12] X.M. Li, Y.H. Zhang, Z.Q. Ma, et al., Chin. Chem. Lett. 30 (2019) 489–493.
[13] Z.H. Yu, Y.C. Guo, H. Dai, et al., Mater. Express 9 (2019) 467–474.
[14] X. Zhang, Y.S. Li, Y.P. Wei, et al., Mater. Express 9 (2019) 808–812.
[15] E. Rideau, R. Dimova, P. Schwille, et al., Chem. Soc. Rev. 47 (2018) 8572–8610.
[16] Y.T. Guntern, J.R. Pankhurst, J. Vávra, et al., Angew. Chem. Int. Ed. 58 (2019) 12632–12639.
[17] L. Chang, Y. Liu, C. Wu, et al., J. Biomed. Nanotechnol. 14 (2018) 786–794.
[18] J. Zhuang, M. Ying, K. Spiekermann, et al., Adv. Mater. 30 (2018) e1804693.
[19] U. Kauscher, M.N. Holme, M. Björnmalm, et al., Adv. Drug Deliv. Rev. 138 (2019) 259–275.
[20] R. Nahire, M.K. Haldar, S. Paul, et al., Biomaterials 35 (2014) 6482–6497.
[21] R.R. Zhang, A.B. Schroeder, J.J. Grudzinski, et al., Nat. Rev. Clin. Oncol. 14 (2017) 347–364.
[22] S. Ye, F. Wang, Z. Fan, et al., ACS Appl. Mater. Interfaces 11 (2019) 15262–15275.
[23] C. Hu, F. Fan, Y. Qin, et al., J. Biomed. Nanotechnol. 14 (2018) 2018–2030.
[24] H.J. Yoon, H.S. Lee, J.Y. Lim, et al., ACS Appl. Mater. Interfaces 9 (2017) 5683–5691.
[25] X. Zheng, D. Xing, F. Zhou, et al., Mol. Pharm. 8 (2011) 447–456.
[26] N. Todorova, C. Chiappini, M. Mager, et al., Nano Lett. 14 (2014) 5229–5237.
[27] Y. Wei, T. Tang, H.B. Pang, Nat. Commun. 10 (2019) 3646.
[28] X. Li, O. Taratula, O. Taratula, et al., Mini Rev. Med. Chem. 17 (2017) 258–267.
[29] H.L. Ma, X.R. Qi, Y. Maitani, et al., Int. J. Pharm. 333 (2007) 177–186.
[30] S.P. Hadipour Moghaddam, J. Saikia, M. Yazdimamaghani, et al., ACS Appl. Mater. Interfaces 9 (2017) 21133–21146.
[31] S.P. Hadipour Moghaddam, M. Yazdimamaghani, H. Ghandehari, J. Control. Release 282 (2018) 62–75.
[32] X. He, J. Zhang, C. Li, et al., Theranostics 8 (2018) 4884–4897.
[33] L. Zhang, Y.M. Zhang, Y. Liu, et al., Chin. Chem. Lett. 30 (2019) 120–122.